Nonswitchable magnetic moments in polycrystalline and (111)-epitaxial permalloy/CoO exchange-biased bilayers

Chen, S.-W.; Lu, X.; Blackburn, Elizabeth; Lauter, Valeria; Ambaye, Hailemariam; Chan, Keith T.; Fullerton, Eric E.; Berkowitz, Ami E.; Sinha, Sunil K.

DOI:
10.1103/PhysRevB.89.094419

Nonswitchable magnetic moments in polycrystalline and (111)-epitaxial permalloy/CoO exchange-biased bilayers

S.-W. Chen,[1,*] X. Lu,[1] E. Blackburn,[2] V. Lauter,[3] H. Ambaye,[3] K. T. Chan,[4] E. E. Fullerton,[4] A. E. Berkowitz,[1,4] and S. K. Sinha[1]

[1]*Department of Physics, University of California, San Diego, La Jolla, California 92093, USA*
[2]*School of Physics and Astronomy, University of Birmingham, B15 2TT, United Kingdom*
[3]*Neutron Sciences Directorate, Oak Ridge National Laboratory, Oak Ridge, Tennessee 37831, USA*
[4]*Center for Magnetic Recording Research, University of California, San Diego, La Jolla, California 92093, USA*

(Received 26 September 2013; revised manuscript received 7 February 2014; published 20 March 2014)

We have measured the interfacial magnetization depth profile in ferromagnet/antiferromagnet exchange-coupled NiFe/CoO bilayers. Both a polycrystalline and an epitaxial-(111) bilayer were examined. We find that the nonswitchable magnetization profile in the biased state is highly correlated with the magnetization profile in the unbiased state. The nonswitchable moment distributions are shown to be consistent with the predictions of a previously reported model for the magnetic and microstructural features of the interfacial region.

DOI: 10.1103/PhysRevB.89.094419 PACS number(s): 75.70.Ak, 75.70.Cn, 61.05.fj

I. INTRODUCTION

When a ferromagnet (FM) and an antiferromagnet (AFM) are exchange coupled through an interface, and are field cooled through the ordering temperature of the AFM, or the FM is deposited below the AFM ordering temperature, the exchange-bias effect (produced by the exchange anisotropy phenomenon) is observed [1]. The exchange-bias effect is characterized by a shift of the hysteresis loop of the FM along the cooling field axis by H_E, the exchange-bias field, usually accompanied by an enhancement of the coercive field H_C. Currently, most magnetic storage systems with thin-film sensors utilize this effect. Since its discovery, there has been a significant research effort to understand the details of the mechanism, and several well-documented reviews have been written in the past decade [2–8]. Yet a complete microscopic understanding of the details in any given AFM/FM bilayer system is still unclear.

Interfacial effects are crucial in the exchange-bias system. Takano *et al.* [9] performed thermoremanent studies on the NiFe/CoO system and suggested a strong correlation between the uncompensated AFM spins and the unidirectional anisotropy. It is now generally accepted that the exchange-bias effect depends strongly on these uncompensated spins (UCSs) at the interface [10]. The shift of the hysteresis loops is produced by those UCSs that are exchange coupled to the magnetic entities in the interfacial region as well as to the AFM. Some of these spins do not reverse completely when the applied field is reversed. We refer to them as nonswitchable (NS) spins. The NS spins include the pinned spins in the AFM layer, as well as the spins coupled to them, which form partial domain walls near the FM-AFM interface [11]. A more detailed discussion about the NS spins is given in the Discussion section. Because the interface is buried, measuring these NS spins is difficult. Penetrating probes, such as x rays and neutrons, are thus some of the limited suitable tools for studying this [12–19]. The problem is further complicated by the differences from system to system [8].

Permalloy (Py)/CoO bilayer is a widely studied exchange-bias system because the ordering temperature of CoO ($T_N \sim$ 290 K) is close to room temperature, the magnetic structure of CoO is well-known, and the soft magnetic properties of Py emphasize exchange-bias effects. There have been several reported studies of this system by various groups. Moran *et al.* [20] studied hysteresis loops of Py films deposited on CoO single crystals with [111] faces and found that increased disorder at the interface increased H_E. They noted that the domain structure of AFM CoO could present a combination of compensated and uncompensated AF spins at the interface. Moran and Schuller [21] studied the dependence of H_E on cooling field and proposed a model where the perpendicular coupling between the AFM and FM spins might be responsible for the exchange bias. Gökemeijer *et al.* [10] carried out magnetization studies of Py deposited on CoO with [111], [110], and [100] faces, respectively, and also on polycrystalline CoO. They found zero values for H_E for the CoO [100] and [110] samples (which are nominally completely compensated), finite but small H_E values for the CoO [111] interface, and larger values for the polycrystalline interface. The coercive field, however, was largest for the [100] sample and smallest for the polycrystalline sample. A recent combined magnetic x-ray scattering and polarized neutron diffraction study by Radu *et al.* [22] relates this behavior to the random orientations of the domains in the (111)-textured system. However, in the previous studies, the nature of the interface magnetization was not studied. This can be studied with resonant magnetic x-ray reflectivity using circular polarization or with polarized neutron reflectivity.

Recent magnetic x-ray reflectivity studies by some of us [23–25] reported that there is a thin interfacial layer in the polycrystalline Py/CoO system which has net Co moments above T_N. The Co moments are pinned antiparallel to the cooling field in the biased state. In this paper, we have extended our previous studies and measured the polarized neutron reflectivity in both polycrystalline and (111)-epitaxial Py/CoO bilayers. The depth profiles of the nonswitchable and switchable components of the magnetization in the vicinity of the Py/CoO interface are obtained and compared, and

*Corresponding author: schen@physics.ucsd.edu

TABLE I. Thickness and roughness of the polycrystalline film and (111)-epitaxial film, obtained by Cu $K\alpha$ x-ray reflectivity measurement. The roughness corresponds to the surface above the layer. SLD is the scattering length density for x rays.

	Polycrystalline film					(111)-epitaxial film			
Layer	Thickness (Å)	Roughness (Å)	SLD (10^{-6} Å^{-2})	Bulk SLD (10^{-6} Å^{-2})	Layer	Thickness (Å)	Roughness (Å)	SLD (10^{-6} Å^{-2})	Bulk SLD (10^{-6} Å^{-2})
Ta_2O_5	34.7	10.4	61.1	54.6	Ta_2O_5	30.0	8.4	56.9	54.6
Ta	30.6	5.5	108.7	104	Ta	29.7	8.5	108.6	104
Py	201.4	10.0	63.6	63.5	Py	206.9	9.8	63.1	63.5
CoO	163.0	6.7	46.5	47.2	CoO	161.8	6.2	47.1	47.2
Si	∞	5.6	20.0	20.1	Al_2O_3	∞	6.0	33.6	33.5

lead to insights into the mechanism of exchange bias in this system.

II. EXPERIMENTS

The polycrystalline Py/CoO bilayer was grown on a Si(100) substrate with the native oxide surface layer. Polycrystalline CoO (∼15 nm) was deposited from a Co target by reactive sputtering in Ar and O_2. The Py (∼20 nm) was deposited from a $Ni_{0.81}Fe_{0.19}$ target in an Ar atmosphere. The sample was capped with Ta (∼4 nm) to prevent oxidation. The (111)-epitaxial bilayer was grown on an Al_2O_3(0001) substrate and had the same thickness as the polycrystalline film. Both samples were characterized by x-ray reflectivity using a Cu $K\alpha$ x-ray unit. The data was fit using a Parratt-type formalism [26], and the fitted structural/chemical profile is listed in Table I. The (111)-epitaxial film was further characterized by x-ray diffraction and shows CoO(111) and Py(111) peaks with Laue oscillations, indicating a high degree of structural order.

The polarized neutron reflectivity measurements were carried out on the Magnetism Reflectometer at beamline 4A of the Spallation Neutron Source, Oak Ridge National Laboratory [27]. The diffuse background was subtracted to obtain the true reflectivity. The samples were first measured at 300 K (above the CoO Néel temperature) in the unbiased state in a 1.15-T in-plane magnetic field. They were then cooled in a 1.15-T or –1.15-T cooling field to 5 K to establish the biased state. The field was cycled three times between ±1.15 T after cooling to minimize any training effects. The reflectivity was measured at both positive and negative saturation states. To measure the reflectivity in the negative saturation state without depolarizing the neutrons, the following methods were applied: (a) measuring at a slightly positive magnetic field after applying a negative saturation field to the sample, and (b) warming up the sample and reversing the direction of the cooling field. The results of the two methods are the same.

To fit the polarized neutron reflectivity, a Parratt-type formalism was used. The nuclear and magnetic parts of the scattering length density profile were uncoupled in the fitting program. The nuclear part was constrained by the Cu $K\alpha$ x-ray reflectivity fitted parameters (Table I) because the x-ray measurements extended to larger Q_z and thus give a better resolution in the structural depth profile. Only the magnetic depth profile was fitted to the polarized neutron data.

The hysteresis loops of both polycrystalline and epitaxial films were measured by a vibrational sample magnetometer (VSM) (Fig. 1). The measuring conditions and the cooling procedure were the same as that of the neutron experiment.

III. RESULTS

The hysteresis loop results (Fig. 1) are consistent with the previous results of Gökemeijer *et al.* [10] The polycrystalline sample has a larger exchange-bias field (H_E) of 87 Oe and an H_C of 178 Oe, while the (111)-epitaxial film has a smaller H_E of 45 Oe but a much larger H_C of 338 Oe. There is a small increase in the saturation magnetization at 5 K compared to that at 300 K, which results mainly from the temperature dependence of the Py moment. In addition, small vertical shifts of the loops are observed at low temperature in both samples, which are attributed to the NS spins, which can exist either at the interface or within the layer [28–30]. The vertical

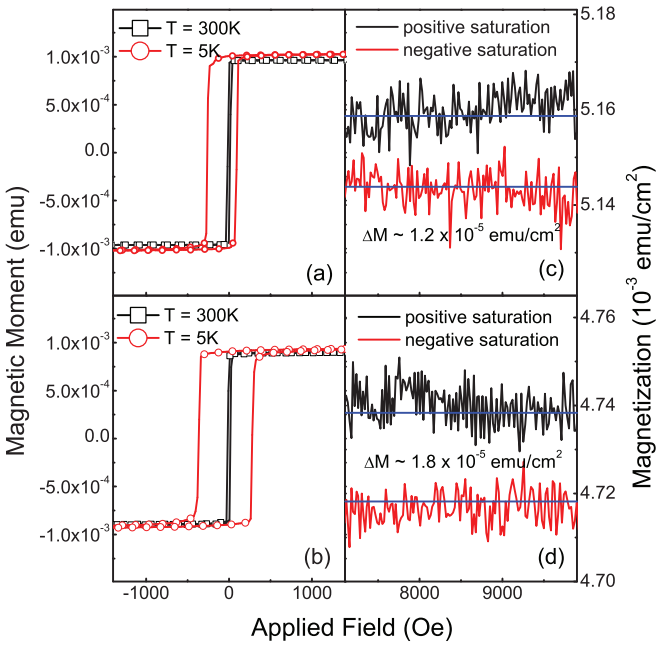

FIG. 1. (Color online) Hysteresis loop of (a) polycrystalline and (b) (111)-epitaxial Py/CoO film at 300 K and after cooling in 1.15-T field to 5 K. A negative exchange bias is observed in both samples. Magnetization at positive and negative saturation applied field (negative flipped for comparison) in (c) polycrystalline film and (d) epitaxial film shows net positive nonswitchable moments in both samples.

shift is determined to correspond to a magnetization of 6.4 × 10^{-6} emu per unit area of film (emu/cm^2) in the polycrystalline sample and 8.8 × 10^{-6} emu/cm^2 in the (111)-epitaxial film [Figs. 1(c) and 1(d)]. Notice that the positive values of the vertical shift indicate that the net NS moment is parallel to the cooling field. The neutron diffraction results showed that the magnetic moment of a Co^{2+} in CoO is approximately 3.8 μ_B [31]. A (111)-Co layer with fully oriented spins in a CoO(111) film can be estimated to be 4.48 × 10^{-5} emu/cm^2. Therefore the net NS magnetization is about 13%–20% of this value. As will be shown later, however, the NS component is not necessarily only from the AFM CoO.

Polarized neutron reflectometry is used to obtain the depth profile of the in-plane magnetization vector [32]. In the reflectometry experiment without the polarization analysis, the measured reflectivities $R^+ = (R^{++} + R^{+-})$ and $R^- = (R^{--} + R^{-+})$ can be fitted individually to obtain the information about the magnetization components parallel and perpendicular to the neutron spin. The perpendicular component is relatively small compared to the parallel component in an in-plane saturation field. In the experiment, the neutron spins were always parallel (spin-up) or antiparallel (spin-down) to the applied field to maintain the polarization. The scattering length density for spin-up and spin-down can be written as $\rho^{\pm\pm}(z) = \rho_n(z) \pm CM(z)$, with $C = 2.853 \times 10^{-9}$ Å^{-2} cm^3/emu, where ρ_n is the nuclear scattering length density and $M(z)$ is the laterally averaged magnetization at depth z. The chemical thickness and roughness are obtained from x-ray reflectivity, so the nuclear part ρ_n is constrained. For the magnetic part, an interfacial layer between Py and CoO was added, which was necessary in order to get a good fit. The magnetic density and the thickness of the Py and the interfacial layer were the fitting parameters, as well as the roughness between the Py/interfacial layer and the interfacial layer/CoO.

Both samples were first measured above the Néel temperature in a saturation field of 1.15 T. Figure 2 shows the fitted polarized neutron reflectivities at 300 K and the structural/magnetic density profiles extracted from the fitting. At 300 K, both samples showed magnetization profiles different from the nuclear profile at the Py-CoO interface. In the polycrystalline case [Fig. 2(c)], the magnetic interfacial roughness is much larger (∼15 Å) than the chemical roughness (∼7 Å) and the magnetization extends into the CoO region. For the (111)-epitaxial film [Fig. 2(d)], a magnetic interfacial layer about 10 Å thick is observed, and its width is within the chemical roughness range.

Polarized neutron reflectivity data were then taken in the exchange-biased state for both samples and for positive and negative saturation fields after cooling to 5 K in a 1.15-T cooling field. Figure 3 shows the results for the asymmetry ratio, defined as $(R^+ - R^-)/(R^+ + R^-)$, and the simulation from the fitting. $(R^+ - R^-)$ measures the nuclear magnetic cross term [32] and is very sensitive to the change in magnetization profile. Figures 4(a) and 4(c) show the magnetic density profiles for the polycrystalline film and the (111)-epitaxial film extracted from the fitting. The magnetization of the film in a saturation field can be expressed as

$$M_{\pm}(z) = M_{NS}^{\pm}(z) \pm M_S(z), \quad (1)$$

where $M_{\pm}(z)$ is the laterally averaged magnetization at depth z, and the positive (negative) sign is for positive (negative) saturation field. The $M_S(z)$ is the switchable component, which completely flips with the magnetic field, and the $M_{NS}^{\pm}$ are the NS components in positive and negative saturation fields, which include the spins that do not switch completely and irreversibly with the field. The depth profile of the net NS part is extracted from $[M_+(z) + M_-(z)]/2$. These are shown for the two samples in Figs. 4(b) and 4(d).

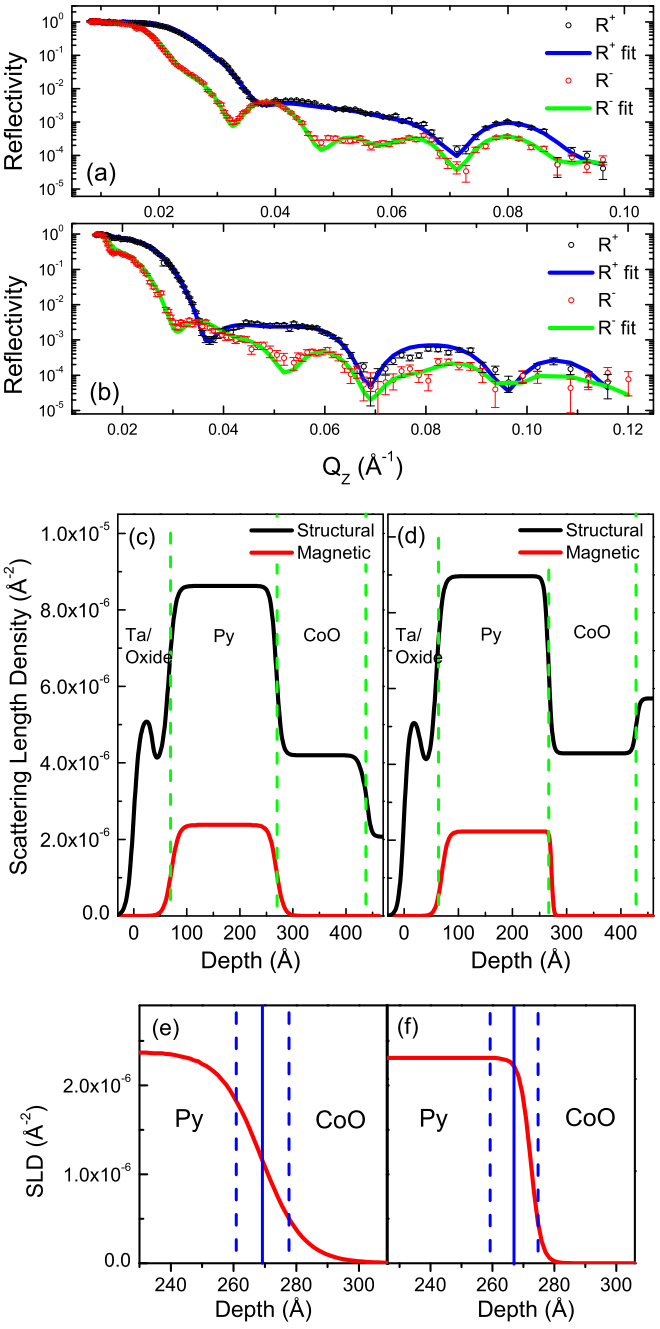

FIG. 2. (Color online) Fitted polarized neutron reflectivity data for (a) polycrystalline film and (b) (111)-epitaxial film at T = 300 K. The structural and magnetic scattering length density profiles extracted from the fitting are shown in (c) and (d), respectively. The green dashed lines define the chemical interfaces. (e), (f) are magnetic density profiles near the Py-CoO interface for polycrystalline and epitaxial film, respectively. The blue solid lines are the chemical interfaces, and the dashed lines indicate the chemical roughness.

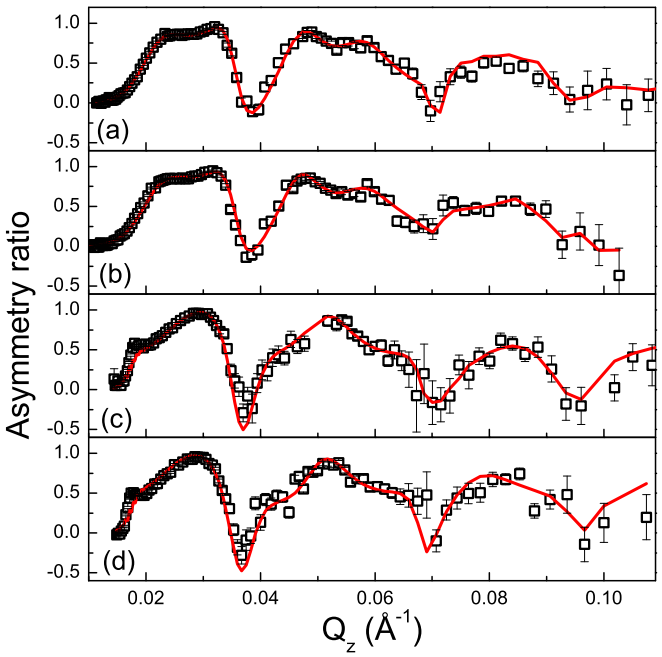

FIG. 3. (Color online) Asymmetry ratio calculated from polarized neutron reflectivity ($T = 5$ K), solid lines are the simulation: (a) polycrystalline film, negative saturation; (b) polycrystalline film, positive saturation; (c) epitaxial film, negative saturation; and (d) epitaxial film, positive saturation.

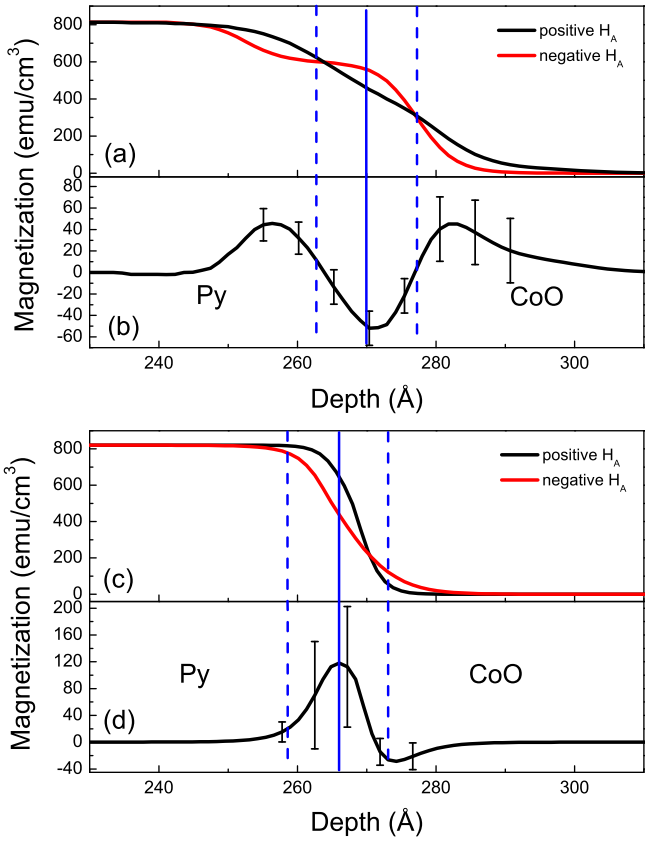

FIG. 4. (Color online) Magnetization profiles at $T = 5$ K extracted from polarized neutron reflectivity fitting: (a) profile of polycrystalline sample and (b) the NS magnetization profile, and (c) profile of epitaxial film and (d) the NS magnetization profile. The blue line is the chemical interface and the dashed lines indicate the chemical roughness.

Note that these measurements were dominated by the components of the magnetization along the direction of the incident neutron polarization which is perpendicular to the scattering plane. The perpendicular components are relatively small and they would require a measurement of the spin-flip reflectivity. These components would be present in the case of a partial domain wall between nonparallel layers of spins (which would presumably form when the magnetization of the ferromagnet was reversed from the direction of the cooling field) and thus the depth profile into the ferromagnet of the measured $M_{NS}(z)$ from a pinned layer at the interface would appear to have a gradually decaying component. Thus $M_{NS}(z)$ in both the ferromagnetic and antiferromagnetic regions are not necessarily fixed magnetization independent of applied field, but could result from the formation of the partial domain walls upon magnetization reversal. This will be discussed in detail in the Discussion section.

A. Polycrystalline film

The NS component of the polycrystalline sample is shown in Fig. 4(b). In the chemical interfacial region, these moments are antiparallel to the cooling field, while in the vicinity of the chemical interface, both the Py and CoO regions show NS moments parallel to the cooling field. This shows that the spins across both interfaces are antiferromagnetically coupled to the spins in the interfacial region, which is in agreement with the resonant soft x-ray results [24]. NS moments exist in both the Py and CoO region about 20 Å on each side, most likely due to partial domain walls originating at the interfaces, as discussed above. At $T = 300$ K [Fig. 2(c)], we observed that there are magnetic moments extending into the CoO region also about 20 Å deep, which could be the origin of these NS spins. NS moment profiles were studied in other exchange-bias bilayers. Brück *et al.* showed that in a MnPd/Fe exchange-bias bilayer, the NS Mn moments extend into MnPd about 13 Å [33]. More recently, Mohanty *et al.* observed that in a NiFe/FeMn bilayer, the NS moments exist in both FM and AFM layers [34]. In the case of our polycrystalline Py/CoO system, the NS moment per unit area is estimated to be $+4.9 \times 10^{-6}$ emu/cm^2, which has the same order of magnitude as the estimate from the hysteresis loop measurement. The switchable part in the biased state is approximately $M_S(z) = [M_+(z) - M_-(z)]/2$. The ratio between the NS moment to the total moment in the interfacial region is about 10% [24,35]. Figure 5 shows the reflectivity and magnetization of this film at $H = 100$ Oe after it was saturated at $H = -1.15$ T. From the hysteresis loop measurement, this is the field where the magnetization is just about to reverse. The magnetization profile [Fig. 5(b)] shows that the reversal starts from the interface instead of coherently flipping throughout the FM film. This indicates that the reversible spins in the FM layer near the interface have a greater tendency to reverse, as they are experiencing the antiferromagnetic coupling to the switchable spins in the interfacial region.

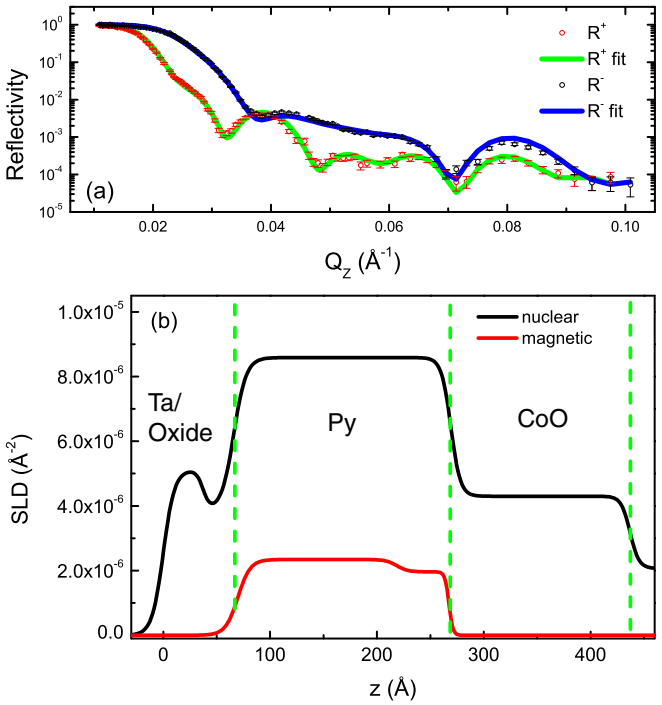

FIG. 5. (Color online) (a) Reflectivity fitting and (b) magnetization profile of the polycrystalline film at $H = +100$ Oe after saturation at $H = -1.15$ T ($T = 5$ K). The magnetization is just about to reverse. The magnetization profile is flipped for a clearer comparison.

B. (111)-epitaxial film

The same analysis procedure was applied to the (111)-epitaxial film. The magnetization profile [Fig. 4(c)] shows that, unlike the polycrystalline sample, the variation is confined to the chemical interfacial region. The NS moments [Fig. 4(d)] are localized in the interfacial region, parallel to the cooling field near the Py side and antiparallel at the CoO side. The NS per unit area is about $+7.6 \times 10^{-6}$ emu/cm^2. The result shows that although the exchange bias is much weaker in a (111)-epitaxial film compared to the polycrystalline bilayer, the magnitude of the NS magnetization is greater. However, the distribution of NS spins is different. In the polycrystalline film, the NS moments exist in both Py and CoO regions as well as the chemical interface. In the (111)-epitaxial film, the NS moments are located at the structural interface and no significant moments are found in the Py and CoO regions. Because the NS moments are only located within a ∼10-Å region and the Q_z range is limited, the uncertainty of the NS moment profile is relatively large for the epitaxial film. The result also shows that the distribution of the NS moments is highly correlated with the magnetization profile of the unbiased state. In the (111)-epitaxial film, we found there is net interfacial magnetization above the Néel temperature within the structural roughness at the interface, and the NS spins are located in the same region in the biased state.

IV. DISCUSSION

Our previous resonant soft x-ray reflectivity studies [24,36] demonstrated the existence of an interfacial region of order 10 Å in the Py-CoO exchange-biased system. At room temperature, above the CoO ordering temperature (T_N), this interfacial region possesses a net magnetization different from that of Py [36]. At 235 K, below T_N, the interfacial layer is still present in the exchange-bias state and contains uncompensated Co magnetization, some of which aligns antiparallel to the cooling field, with the major portion oriented parallel to an applied field [24]. The present neutron data shows the distribution of the NS magnetization for both polycrystalline and epitaxial Py-CoO bilayers. This extensive data facilitates the development of a model of the magnetic microstructure of the interfacial region, which was recently discussed in Ref. [25].

The model includes an attempt to reproduce and characterize the ∼10-Å interfacial region and to examine its influence on the properties of the bilayers with thicker Py. The hysteresis loop of a Py(1 nm)/CoO(50 nm) bilayer, which simulated the interfacial layer, clearly indicates that the interfacial region consists of a very hard magnetic phase and a very soft component [25]. Further analysis showed that the hard phase was composed of $CoFe_2O_4$ nanoparticles exchange-coupled to the CoO, and that the soft component was composed of nanoparticles that were not exchange-coupled to either the CoO or the Py. Thus, the coupling of the Py to the CoO was mediated by the $CoFe_2O_4$ nanoparticles. The presence of $CoFe_2O_4$ in the interfacial region results from the oxidation or reduction reactions that occur at the interfaces of CoO with Fe, Co, or Ni [37,38]. It was shown that the dependence of H_C and H_E on Py thickness and on temperature, as well as the magnitude of $\Delta\sigma$ (interfacial energy difference between the two ferromagnetic orientations) in Malozemoff's expression for the exchange interaction [39,40],

$$H_E = \frac{\Delta\sigma}{2M_S t}, \tag{2}$$

could be derived from an ∼10-Å interfacial region consisting of $CoFe_2O_4$ and soft nanoparticles, as described above [25]. Since this represents the most comprehensive description of an exchange-bias system available, it is pertinent to examine whether this magnetic microstructure of the interfacial region can explain the NS magnetization distributions in Fig. 4. Consideration of this model [25] recognizes that there is an intermediate layer between the CoO and Py, and that the exchange bias between the CoO and Py layers is mediated by $CoFe_2O_4$ nanoparticles in this layer, i.e., the $CoFe_2O_4$ nanoparticles are pinned to UCSs in the CoO and are exchange coupled to the Py spins, thereby transmitting the bias to the Py. The bias is provided by reversible partial domain walls in the CoO at interfaces with the $CoFe_2O_4$ nanoparticles. As discussed above, UCSs are responsible for H_E, and it was shown that the uncompensated spin density is inversely proportional to AFM crystallite size [9]. A higher H_E is therefore expected with polycrystalline as compared with epitaxial CoO as a consequence of the higher uncompensated spin density. It is relevant to note that Radu *et al.* [22] concluded that UCSs are responsible for H_E also in their (111)-epitaxial bilayer, CoO(200 nm)-Py(12 nm). The temperature dependencies of H_E and H_C in that bilayer were the same as for the polycrystalline samples in Ref. [25]. H_E was smaller in the epitaxial bilayer in Ref. [22] than in our epitaxial bilayer,

as expected from lesser constraints on partial walls in the much thicker epitaxial CoO. These comparisons suggest a similar interfacial structure in the epitaxial bilayer as in the polycrystalline one. What remains to be explained is the larger H_C in the epitaxial bilayer. That CoO domain behavior is involved in the epitaxial H_C can be inferred from the much larger value for the 200-nm CoO [22] than in our ∼20-nm CoO. This indicates some irreversible changes in the epitaxial CoO domain state after applied field reversal. Such changes were indeed found by polarized neutron diffraction studies by Radu *et al.* [22]. Thus we may conclude that the increased H_C in the epitaxial bilayer is provided by irreversible CoO domain changes as the $CoFe_2O_4$ nanoparticles to which they are coupled are reversed by the applied field. It is expected that such irreversible CoO domain changes are much smaller or absent in the polycrystalline sample due to pinning at the grain boundaries of the CoO crystallites.

There are four cases to be considered, $CoFe_2O_4$-CoO interaction, AFM and FM, with $CoFe_2O_4$-Py interaction, AFM and FM. By inspecting the NS magnetization profile in Fig. 4(b), it is reasonable to assume both $CoFe_2O_4$-CoO and $CoFe_2O_4$-Py are AFM coupled. In our model, the NS spins include the following components: (1) Some of the UCSs in CoO which are strongly exchange coupled to the bulk CoO spins and are pinned in the cooling field direction. These are the spins which ultimately give rise to the exchange bias. (2) The spins in the ferrite nanoparticles which are AFM coupled to both Py and CoO spins and are thus antiparallel to the cooling field. (3) The CoO spins at the interface which form partial domain walls between pinned CoO and the ferrite spins. (4) The Py spins at the interface which form partial domain walls between bulk Py and the ferrite spins. Note that there are also unpinned UCS CoO spins and spins in the ferrite nanoparticles that are not coupled to CoO and Py spins. These spins do not contribute to the NS magnetization and are responsible for the enhancement of the coercive field. Figure 6 shows the schematics of the NS spin components and the sum of H↑ and H↓ reproduces the polycrystalline sum in Fig. 4(b). The AFM interaction between Py and $CoFe_2O_4$ causes frustration of the Py spins at the interface, which explains why the Py spins at the interface have a greater tendency to reverse. For the epitaxial bilayer, the exchange interaction between CoO and the $CoFe_2O_4$ is again AFM but with a big difference in magnetization profile at the interface from the polycrystalline bilayer. For the epitaxial case, the uncompensated spin density is significantly lower [9] than that in the polycrystalline. Therefore, the epitaxial $CoFe_2O_4$ nanoparticles are the principal components which respond to the cooling field. They were magnetized in the cooling field direction and the adjacent CoO spins adjusted to this condition with AFM coupling, which results in the small negative dip at the CoO interface, as shown in Fig. 4(b).

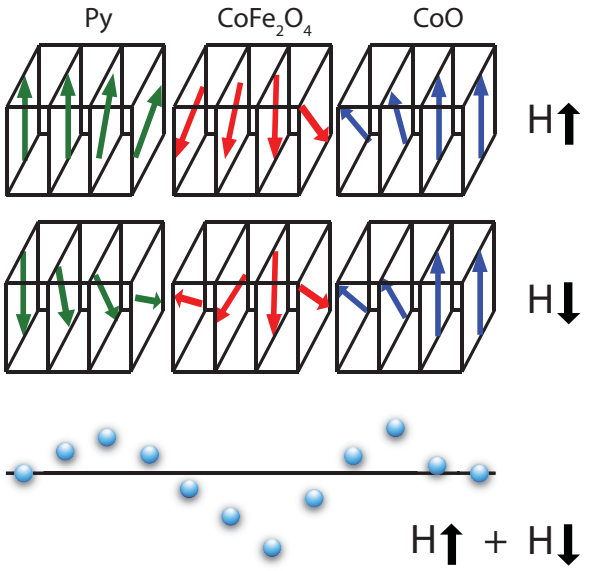

FIG. 6. (Color online) The schematic of the spin configuration in the polycrystalline sample in a positive and negative saturation field. Every other plane of the CoO is shown for clarity. The sum of the two (blue spheres) yields the net NS moment profile, which reproduces the experimental observation.

V. CONCLUSION

Both a polycrystalline and a (111)-epitaxial Py/CoO bilayer were examined by polarized neutron reflectometry. We confirmed that there are interfacial net magnetic moments above the Néel temperature, and the location of the net nonswitchable spins are highly related to these spins. The net nonswitchable moments in the polycrystalline bilayer exist in both Py and CoO layers, and the moments in the epitaxial bilayer are only localized at the interfacial region. A previously proposed model based on a 10-Å interfacial layer consisting of $CoFe_2O_4$ nanoparticles was examined. The nonswitchable magnetization profile derived from the model successfully reproduces the profiles in both bilayers, assuming an AFM coupling between the moments in CoO and $CoFe_2O_4$.

ACKNOWLEDGMENT

This work at UCSD, including experiments at ORNL, was supported by Basic Energy Sciences, US Department of Energy, under Grant No. DE-SC0003678.

[1] W. H. Meiklejohn and C. P. Bean, Phys. Rev. **105**, 904 (1957).
[2] J. Nogués and I. K. Schuller, J. Magn. Magn. Mater. **192**, 203 (1999).
[3] A. E. Berkowitz and K. Takano, J. Magn. Magn. Mater. **200**, 552 (1999).
[4] R. L. Stamps, J. Phys. D Appl. Phys. **33**, R247 (2000).
[5] M. Kiwi, J. Magn. Magn. Mater. **234**, 584 (2001).
[6] J. Nogués, J. Sort, V. Langlais, V. Skumryev, S. Suriñach, J. Muñoz, and M. Baró, Phys. Rep. **422**, 65 (2005).

[7] A. E. Berkowitz and R. H. Kodama, in *Nanomagnetism: Ultrathin Films, Multilayers and Nanostructures*, edited by D. Mills and J. Bland, Contemporary Concepts of Condensed Matter Science (Elsevier Science, New York, 2006), pp. 115–152.
[8] F. Radu and H. Zabel, in *Magnetic Heterostructures*, edited by H. Zabel and S. Bader, Springer Tracts in Modern Physics Vol. 227 (Springer, Berlin, 2008), p. 97.
[9] K. Takano, R. H. Kodama, A. E. Berkowitz, W. Cao, and G. Thomas, Phys. Rev. Lett. **79**, 1130 (1997).
[10] N. J. Gökemeijer, R. L. Penn, D. R. Veblen, and C. L. Chien, Phys. Rev. B **63**, 174422 (2001).
[11] D. Mauri, H. C. Siegmann, P. S. Bagus, and E. Kay, J. Appl. Phys. **62**, 3047 (1987).
[12] M. R. Fitzsimmons, P. Yashar, C. Leighton, I. K. Schuller, J. Nogues, C. F. Majkrzak, and J. A. Dura, Phys. Rev. Lett. **84**, 3986 (2000).
[13] C. Leighton, M. R. Fitzsimmons, P. Yashar, A. Hoffmann, J. Nogués, J. Dura, C. F. Majkrzak, and I. K. Schuller, Phys. Rev. Lett. **86**, 4394 (2001).
[14] H. Ohldag, T. J. Regan, J. Stöhr, A. Scholl, F. Nolting, J. Lüning, C. Stamm, S. Anders, and R. L. White, Phys. Rev. Lett. **87**, 247201 (2001).
[15] M. Gierlings, M. J. Prandolini, H. Fritzsche, M. Gruyters, and D. Riegel, Phys. Rev. B **65**, 092407 (2002).
[16] A. Hoffmann, J. W. Seo, M. R. Fitzsimmons, H. Siegwart, J. Fompeyrine, J.-P. Locquet, J. A. Dura, and C. F. Majkrzak, Phys. Rev. B **66**, 220406 (2002).
[17] F. Radu, M. Etzkorn, R. Siebrecht, T. Schmitte, K. Westerholt, and H. Zabel, Phys. Rev. B **67**, 134409 (2003).
[18] M. R. Fitzsimmons, B. J. Kirby, S. Roy, Z.-P. Li, I. V. Roshchin, S. K. Sinha, and I. K. Schuller, Phys. Rev. B **75**, 214412 (2007).
[19] J. Wu, J. S. Park, W. Kim, E. Arenholz, M. Liberati, A. Scholl, Y. Z. Wu, C. Hwang, and Z. Q. Qiu, Phys. Rev. Lett. **104**, 217204 (2010).
[20] T. Moran, J. Gallego, and I. K. Schuller, J. Appl. Phys. **78**, 1887 (1995).
[21] T. J. Moran and I. K. Schuller, J. Appl. Phys. **79**, 5109 (1996).
[22] F. Radu, S. Mishra, I. Zizak, A. Erko, H. Dürr, W. Eberhardt, G. Nowak, S. Buschhorn, H. Zabel, K. Zhernenkov *et al.*, Phys. Rev. B **79**, 184425 (2009).
[23] S. Roy, M. Fitzsimmons, S. Park, M. Dorn, O. Petracic, I. Roshchin, Z.-P. Li, X. Batlle, R. Morales, A. Misra *et al.*, Phys. Rev. Lett. **95**, 047201 (2005).
[24] E. Blackburn, C. Sanchez-Hanke, S. Roy, D. J. Smith, J. I. Hong, K. T. Chan, A. E. Berkowitz, and S. K. Sinha, Phys. Rev. B **78**, 180408 (2008).
[25] A. E. Berkowitz, J. I. Hong, S. K. McCall, E. Shipton, K. T. Chan, T. Leo, and D. J. Smith, Phys. Rev. B **81**, 134404 (2010).
[26] L. Parratt, Phys. Rev. **95**, 359 (1954).
[27] V. Lauter, H. Ambaye, R. Goyette, W.-T. H. Lee, and A. Parizzi, Physica B **404**, 2543 (2009).
[28] J. Nogués, C. Leighton, and I. K. Schuller, Phys. Rev. B **61**, 1315 (2000).
[29] H. Ohldag, A. Scholl, F. Nolting, E. Arenholz, S. Maat, A. T. Young, M. Carey, and J. Stöhr, Phys. Rev. Lett. **91**, 017203 (2003).
[30] E. C. Passamani, C. Larica, C. Marques, J. R. Proveti, A. Y. Takeuchi, and F. H. Sanchez, J. Magn. Magn. Mater. **299**, 11 (2006).
[31] W. L. Roth, Phys. Rev. **110**, 1333 (1958).
[32] M. Fitzsimmons and C. Majkrzak, in *Modern Techniques for Characterizing Magnetic Materials*, edited by Y. Zhu (Kluwer, Boston, 2005), pp. 107–152.
[33] S. Brück, G. Schütz, E. Goering, X. Ji, and K. M. Krishnan, Phys. Rev. Lett. **101**, 126402 (2008).
[34] J. Mohanty, A. Persson, D. Arvanitis, K. Temst, and C. Van Haesendonck, New J. Phys. **15**, 033016 (2013).
[35] J. van Lierop, B. W. Southern, K.-W. Lin, Z.-Y. Guo, C. L. Harland, R. A. Rosenberg, and J. W. Freeland, Phys. Rev. B **76**, 224432 (2007).
[36] S. Roy, C. Sanchez-Hanke, S. Park, M. Fitzsimmons, Y. Tang, J. Hong, D. Smith, B. Taylor, X. Liu, M. Maple *et al.*, Phys. Rev. B **75**, 014442 (2007).
[37] R. F. C. Farrow, M. J. Carey, R. F. Marks, P. M. Rice, and D. J. Smith, Appl. Phys. Lett. **77**, 1191 (2000).
[38] T. J. Regan, H. Ohldag, C. Stamm, F. Nolting, J. Lüning, J. Stöhr, and R. L. White, Phys. Rev. B **64**, 214422 (2001).
[39] A. P. Malozemoff, Phys. Rev. B **35**, 3679 (1987).
[40] A. P. Malozemoff, J. Appl. Phys. **63**, 3874 (1988).